MATERIALS SCIENCE

Food LEGO: Building hollow cage and sheet superstructures from starch

Arkaye Kierulf^{1,2}, Imann Mosleh¹†, Jieying Li¹†, Peilong Li¹, Amin Zarei¹, Leila Khazdooz¹, James Smoot², Alireza Abbaspourrad¹*

The idea of building large structures from small building blocks has had a long history in the human imagination, from the beautifully intricate shells assembled from silica by unicellular algae to the Egyptian pyramids built from stone. Carrying this idea into the food industry has important implications. Here, we introduce a Pickering emulsion platform for building superstructures like hollow cages and sheets using starch granules as building blocks. In food, these superstructures occupy up to six times more space than their constituent parts, thereby delivering a viscosity greater by an order of magnitude than unstructured starch. To achieve this higher viscosity, they use an alternative superstructure mechanism as opposed to the classic swelling mechanism of individual particles. These super-thickeners may reduce calories, cut production costs, and stretch the global food supply, demonstrating how we can design the future by playing with our food.



NonCommercial

License 4.0 (CC BY-NC).

INTRODUCTION

Throughout history, we have been captivated not only by how nature builds superstructures from small building blocks but also by how these superstructures provide a functional beauty. Large structures, we learn, are more than just a sum of their parts. Just as the rich tapestry of Anglophone literature is composed of only 26 letters, so our DNA is assembled from only four nucleotides. For millions of years, unicellular algae have constructed beautifully intricate shells to house themselves from nothing but silica, with a honeycomb pattern of pores that makes them lightweight but strong (Fig. 1) (1, 2). Inspired by these unexpected properties, many have tried building superstructures at varying length scales. On the scale of several hundred meters, by layering stone blocks, Egyptians built the Great Pyramids, which have survived thousands of years. At the other end of the spectrum, chemists have fused 60-carbon icosahedral cages called Buckminsterfullerenes or "Bucky balls" at the nanoscale (3). These cages were found to have both high optical absorption and high antioxidant activity, making them prime materials for solar cells (4) and antiaging drugs (5). Recently, physicists have even stacked oneatom-thick graphene sheets on top of each other to make superlattices. These carbon sheets exhibit a tunable superconductivity, considered by many as the holy grail of condensed matter physics and regarded as vital to the development of quantum computers (6).

Here, we report the development of a platform to make superstructures from carbohydrates at the micrometer scale and the investigation of their properties in food. We define superstructures as large, stand-alone structures assembled from small, identical (or almost identical) building blocks in such a way that the whole exhibits properties distinct from its constituent parts. Our platform will contribute to the revolution that is now sweeping the food industry as it seeks to address a myriad of issues. Innovations like plant-based meat alternatives and three-dimensionally (3D)-printed snacks with hunger-satiating patterns are being offered as solutions to global concerns over food supply, sustainability, obesity, and diet-triggered diseases (7–9). Starch, oil, and salt, all favorite kitchen staples, but a bane to our collective health when added in excess, are being replaced with healthier alternatives. One such alternative is the salt microsphere. It delivers the same intensity of saltiness but, because it is hollow inside, reduces salt intake by as much as 50% (10). Extending the success of these salt microspheres, we fabricated hollow cages and sheets from starch.

Starch is a staple texturizer used in food products around the world. The ability of starches to swell when heated or sheared provides food manufacturers with a tool to fine-tune both texture and taste, the holy grails of food science. Starch makes breakfast yogurts creamy, lunch soups thick, and dinner desserts jiggly. The classic starch swelling mechanism that allows for this control works at the granular level. Individual starch granules swell and occupy a larger effective volume than is dictated by their mass, which causes them to jam against each other, restricting the flow of the food matrix and increasing viscosity (11).

Starch superstructures follow an alternative mechanism that works at the supragranular level. Because starch hollow cages are empty inside, and starch sheets can cascade on top of each other and trap spaces in between them, their inflated volume restricts the flow of the food matrix and boosts viscosity. This means that the amount of starch required to achieve a food's desirable viscosity, texture, and taste is reduced. This opens the door to making reduced-calorie food products that benefit consumer health, cut costs for food manufacturers, and ease the strain on the global food supply.

The platform we developed owes its inception to the rising field of Pickering emulsions (see section S1 for a brief literature survey) (12–17). Like small-molecule emulsifiers, solid particles such as moderately hydrophobic starch granules can lodge themselves around an oil droplet and stabilize a specific type of emulsion called a Pickering emulsion (18). Pickering emulsions have been used in the cleanlabel encapsulation of bioactive compounds and in the formulation of egg-free and gluten-free products (12). Recently, it was found that if such starch-stabilized emulsions were briefly heat treated, partial gelatinization of the starch granules occurs around the droplet. This partial gelatinization fuses the granules together and improves their encapsulation properties (19, 20). Using this pivotal work as a starting

¹Department of Food Science, College of Agriculture and Life Sciences, Cornell University, 243 Stocking Hall, Ithaca, NY 14853, USA. ²Tate & Lyle Solutions USA LLC, 5450 Prairie Stone Pkwy, Hoffman Estates, IL 60192, USA.

^{*}Corresponding author. Email: alireza@cornell.edu

[†]These authors contributed equally to this work.

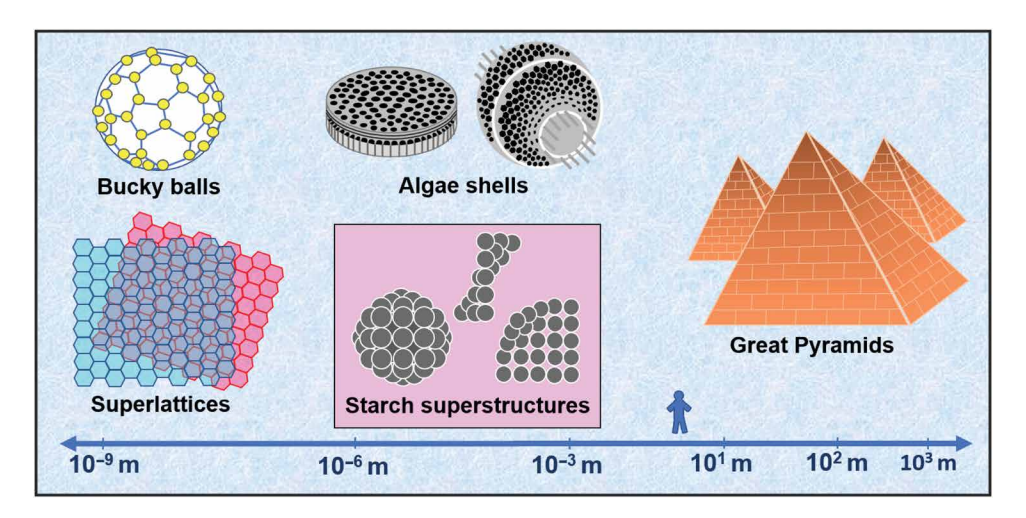


Fig. 1. Superstructures built from small building blocks at different length scales.

point, we developed a platform to generate superstructures of different shapes and sizes, specifically 2D sheets and 3D hollow cages, using amaranth starch as a LEGO-like building block. We then investigated the structure and properties of these sheets and cages and assessed their potential application as super-thickeners in food.

RESULTS

We built superstructures using amaranth starch granules as building blocks via a Pickering emulsion approach (Fig. 2A). We first extracted amaranth starch from amaranth flour in such a way that we retained some native proteins. The small size (~1 µm), high protein content (2.4%), and tunable softness of this high-protein amaranth starch make it the best candidate for building fused superstructures using this approach, and was therefore used as our building block for the entire study (21). These high-protein starch granules, being moderately hydrophobic, will position themselves around an oil droplet at the oil/water (O/W) interface during emulsification via high-shear homogenization [Fig. 2A(2)] (21). If no heat treatment is conducted after emulsification, and we remove both the inner (oil) and outer (water) phases by freeze-drying, the adjacent starch granules that originally surrounded the oil droplet will peel off into 2D sheets [Fig. 2A(3a)], which can then be cross-linked to reinforce them [Fig. 2A(4a)]. The size of these sheets can be controlled; for example, by increasing the homogenization speed, smaller oil droplets are formed, which reduce the size of the sheets. Alternatively, if controlled heating is briefly applied after emulsification, but before freeze-drying, adjacent starch granules surrounding the oil droplet become fused together to form a strong hollow 3D cage after removal of both the inner and outer phases [Fig. 2A(3b)], which can then also be crosslinked [Fig. 2A(4b)]. We investigated these superstructures in terms of their morphology, spatial and structural (molecular) conformation, water-holding capacity (WHC), critical caking concentration (CCC), and viscosity, along with the effect of method parameters such as heating temperature and heating time on cage morphology and crystallinity.

Morphology by SEM

The Pickering emulsion–based method developed here is versatile: After the starch granules have been made to surround an oil droplet, without heat treatment, the method produces sheets (~100% estimated

yield) (Fig. 2, B and C), and with heat treatment, it produces hollow cages (54–83% estimated yield of intact cages) (Fig. 2D).

Without heating, the adjacent starch granules that cover the oil droplets are not well fused together and thus readily break off into sheets when the oil and water phases are removed, like peeling the skin off an onion. Large Pickering emulsions, made using a low homogenization speed (11 k rpm), break into large sheets 10 μm or longer (Fig. 2B). When higher homogenization speeds are used (22 k rpm), small Pickering emulsions that break into smaller sheets less than 10 μm in length are made (Fig. 2C). By increasing the homogenization speed, we are adding more kinetic energy to the system to split up large droplets into smaller droplets. By controlling the homogenization speed, we control the oil droplet size, and, by extension, we control the size of the sheets formed.

Applying heat briefly allows the adjacent starch granules on the surface of the oil droplets to soften and fuse tightly with each other. These inter-granule connections are further strengthened via crosslinking to produce hollow cages that generally remain intact even after the oil and water phases have been removed (Fig. 2D). Hollow cages are the predominant form after heating (54-83%), but a small percentage of sheets do form because of cage breakup or collapse. A range of Pickering emulsion droplet sizes are usually present after homogenization and before heat treatment, so both small and large cages are formed. Small cages with diameters at or below 10 µm typically remain intact and thus exist as the predominant form (Fig. 3, A and B, blue arrows), while large cages with diameters greater than 10 µm tend to collapse (Fig. 3, A and B, red arrows) or break into sheets (Fig. 3, C and D, yellow arrows). Smaller cages are more stable than larger cages: We can find parallels in the architecture of domes and arches, where smaller radii of curvature impart greater architectural strength. Magnification of a single intact cage shows that while the starch granules are partially gelatinized by heat and fused together, they do retain their granular integrity (Fig. 3, E and F). Fully gelatinized starch particles heated for a longer time would have lost their granular shape entirely (see section S2 and fig. S1 for effect of heating parameters on cage morphology). Holes were also observed on the cages. We believe that these holes were made when the oil droplet escaped during freeze-drying; it is through these holes that we can see and verify that the cages are hollow (Fig. 3, G and H, green arrows).

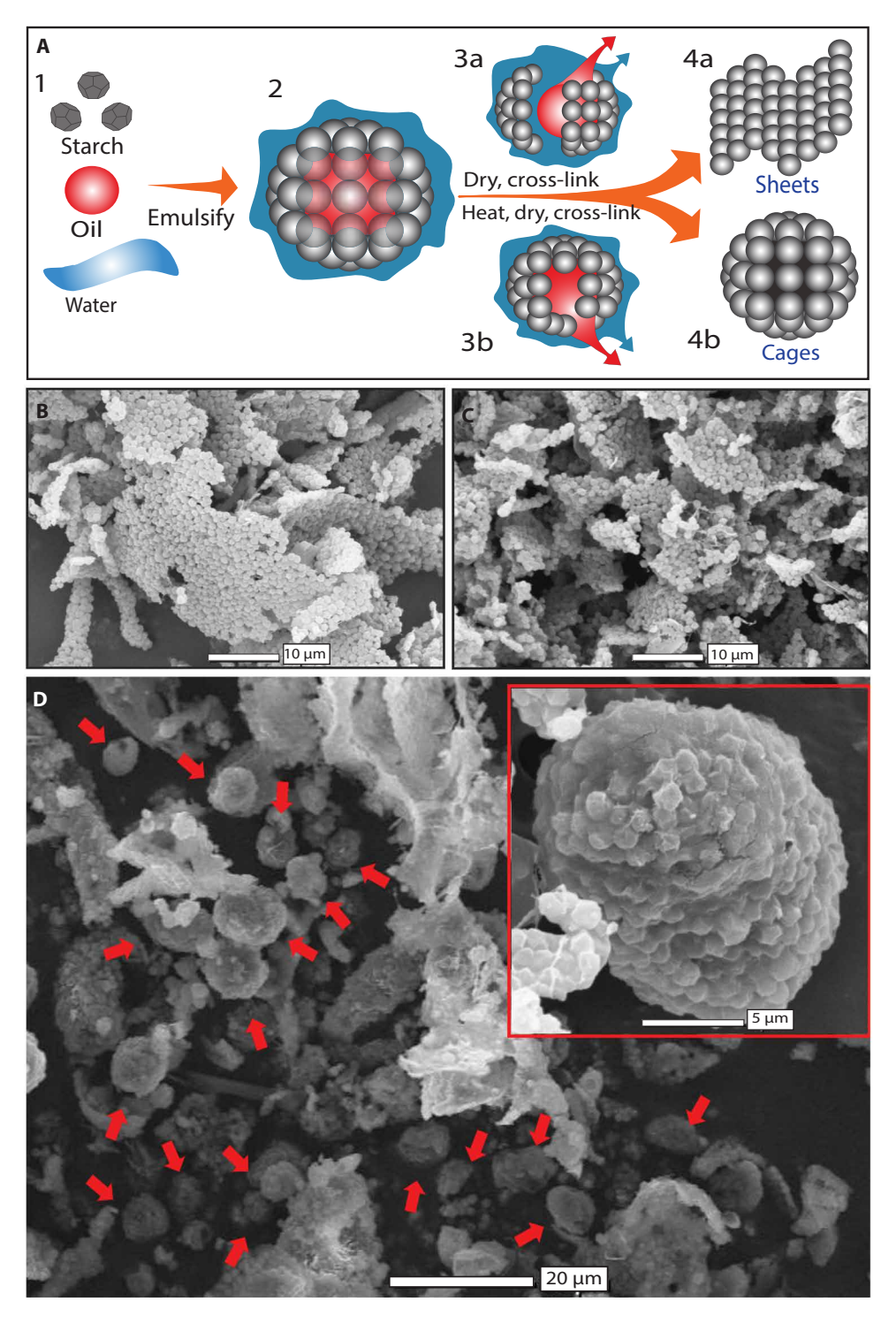


Fig. 2. Schematic for making starch superstructures. (A) Method schematic; SEM images of (B) large sheets (>10- μ m lengths), (C) small sheets (<10- μ m lengths), and (D) hollow cages (~10 μ m in diameter). In (D), red arrows point to cages, and inset is one cage magnified.

Spatial conformation of starch superstructures

By looking closer at these superstructures using field-emission scanning electron microscopy (FE-SEM), we can further elucidate their spatial orientation (Fig. 4A). Unmodified amaranth starch granules are generally polygonal in shape, similar to a dodecahedron, with sharp edges (Fig. 4B); however, when we make starch sheets, even

without heat treatment, the process gently softens the outer layer of the granules, rounding out their edges (Fig. 4, C and D). We also observe narrow bridges (red arrows) at the contact points between adjacent granules, fusing them together loosely. For cages, however, because they undergo a brief heat treatment, the granules appear even softer and the edges more rounded (Fig. 4E). The granules

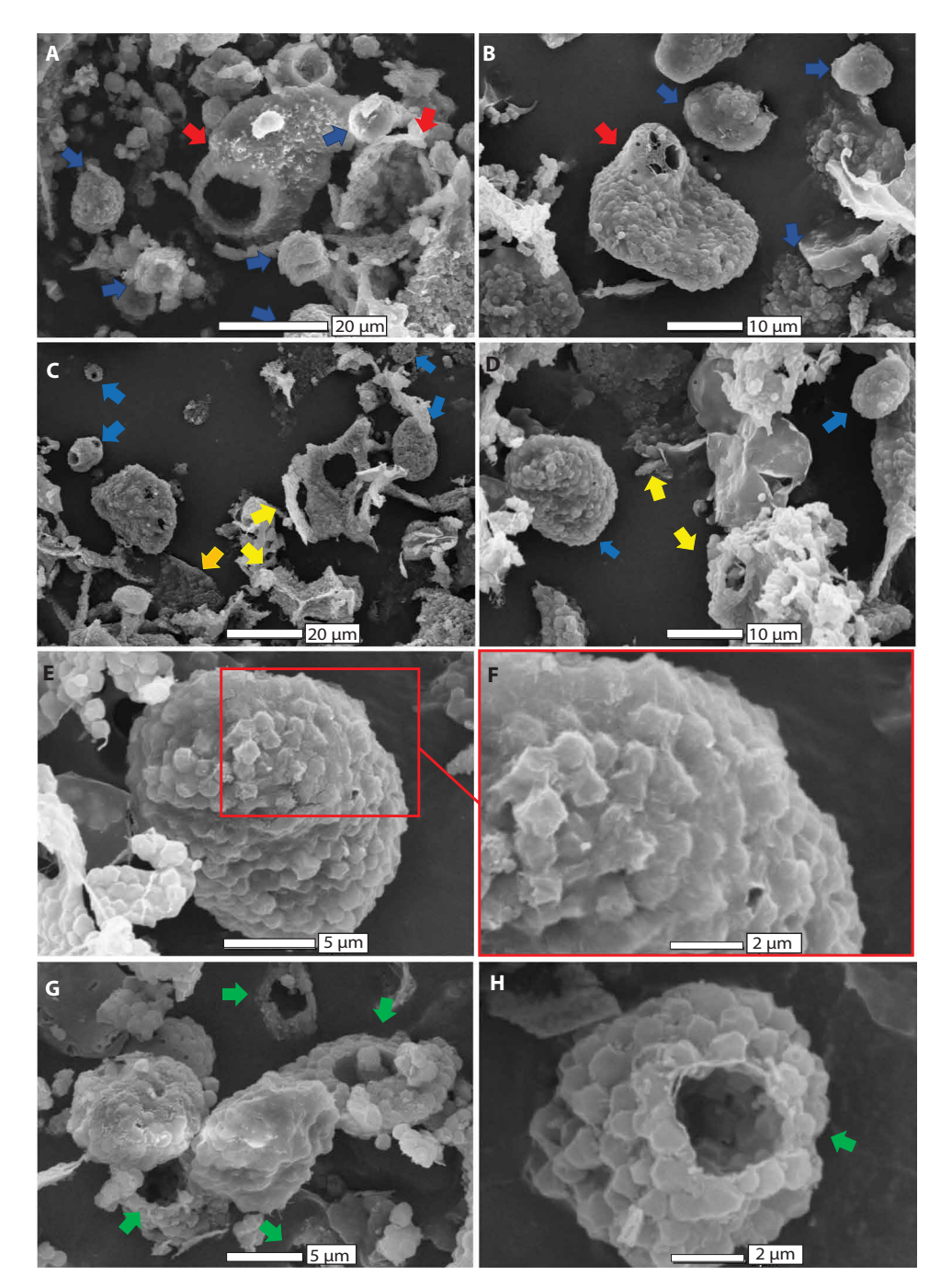


Fig. 3. Morphology of starch hollow cages. SEM images of (A and B) large and small cages, (C and D) sheets, (E and F) one hollow cage, and (G and H) holes on the cages. Arrows are color coded as follows: blue (small cages), red (large cages), yellow (sheets), and green (holes).

overlap, indicating a tight fusion, which suggests that cages may remain more intact than sheets. It is possible, however, that a mixture of tight and loose fusion may coexist in these superstructures, specifically in the case of cages, due to variations in the diffusion of heat during synthesis.

In addition, we postulated that the adjacent granules forming the sheets would be fused together at an angle of about 180°. We observe under SEM that while sheets are generally flat as we postulated, they

are flexible and can fold up or down, with angles even below 90° (Fig. 4, F and G). By approximating the cross-sectional geometry of a 10- μ m cage as a 31-sided polygon, we further postulated that when the granules formed cages, they would curve at a narrower angle of about 168° . Their actual curvature comes close to this (Fig. 4H), and while cages have less freedom of motion than sheets, they do have some variation in their angle of curvature depending on their size and shape.

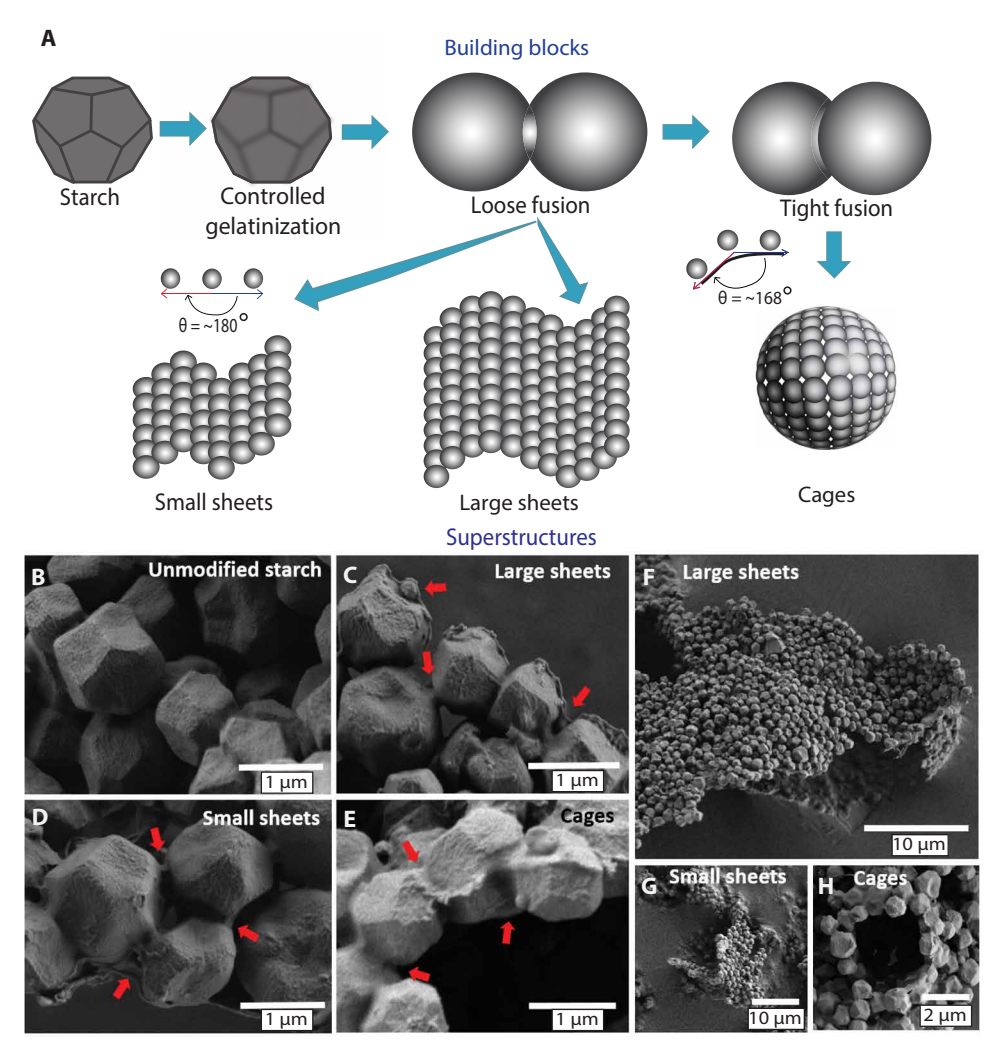


Fig. 4. Spatial conformation of starch superstructures. (A) Spatial schematic; close-up FE-SEM images of (B) unmodified starch, (C) large sheets, (D) small sheets, and (E) cages. Zoom-out FE-SEM images showing the curvature of (F) large sheets, (G) small sheets, and (H) cages.

Structural conformation of starch superstructures: Granular fusion

In addition to their spatial conformation, we also looked at how these superstructures are constructed at the molecular level (Fig. 5A). Unmodified starch granules are made up of chains of glucose that originate from the center of the granule and extend outward to the surface, either linearly (amylose) or as branches (amylopectin). These chains extend outward in the form of random coils, single helices, or double helices, depending on how the chains are ordered and packed together, creating concentric rings of crystalline and amorphous regions akin to the growth-rings of trees (22, 23). As the individual granules soften, fuse, and stitch together to build superstructures, their internal molecular structure will change, and this change affects the superstructure's stability and, by extension, its properties.

X-ray diffraction

To investigate the long-range molecular order at the scale of crystals inside the starch granule, we used x-ray diffraction (XRD). The XRD pattern of unmodified amaranth starch exhibits sharp crystalline peaks at 15°, 17.5°, and 23.5°, with a relative crystallinity (C%) of 33% (Fig. 5B) (24). This indicates that 33% of its chains are tightly

packed together in an A-type crystal arrangement, while the rest are disordered or amorphous. As we then start fusing the granules together to make large and small sheets, C% decreases to 26 and 27%, respectively. Likewise, control 1 (prepared with no emulsification and no heating) shows a decrease in C% down to 31%. As we form sheets, even without heating, the native starch's crystallinity is reduced; we attribute this to solvent, freeze-drying, or dryheat cross-linking effects. Moreover, the hollow cages show a much lower C% of 22%, and so did control 2 (no emulsification, but heated, C% = 24%).

Amaranth starch has a peak gelatinization temperature of 73°C, which means that when heated at this temperature for about 20 min, most crystals will melt, resulting in full gelatinization (25). To make the cages, we performed a brief heat treatment at 75°C but only held the samples at that temperature for 3 min—long enough to partially gelatinize the starch granules but not long enough for full gelatinization. Brief heating accomplishes two things: One, it softens the granules, loosening the amylopectin and amylose chains on the surface, which facilitates chain entanglement between adjacent granules and fuses them together into the cage structure; two, the short 3-min heating time prevents a complete loss of crystallinity. The fused granules retain

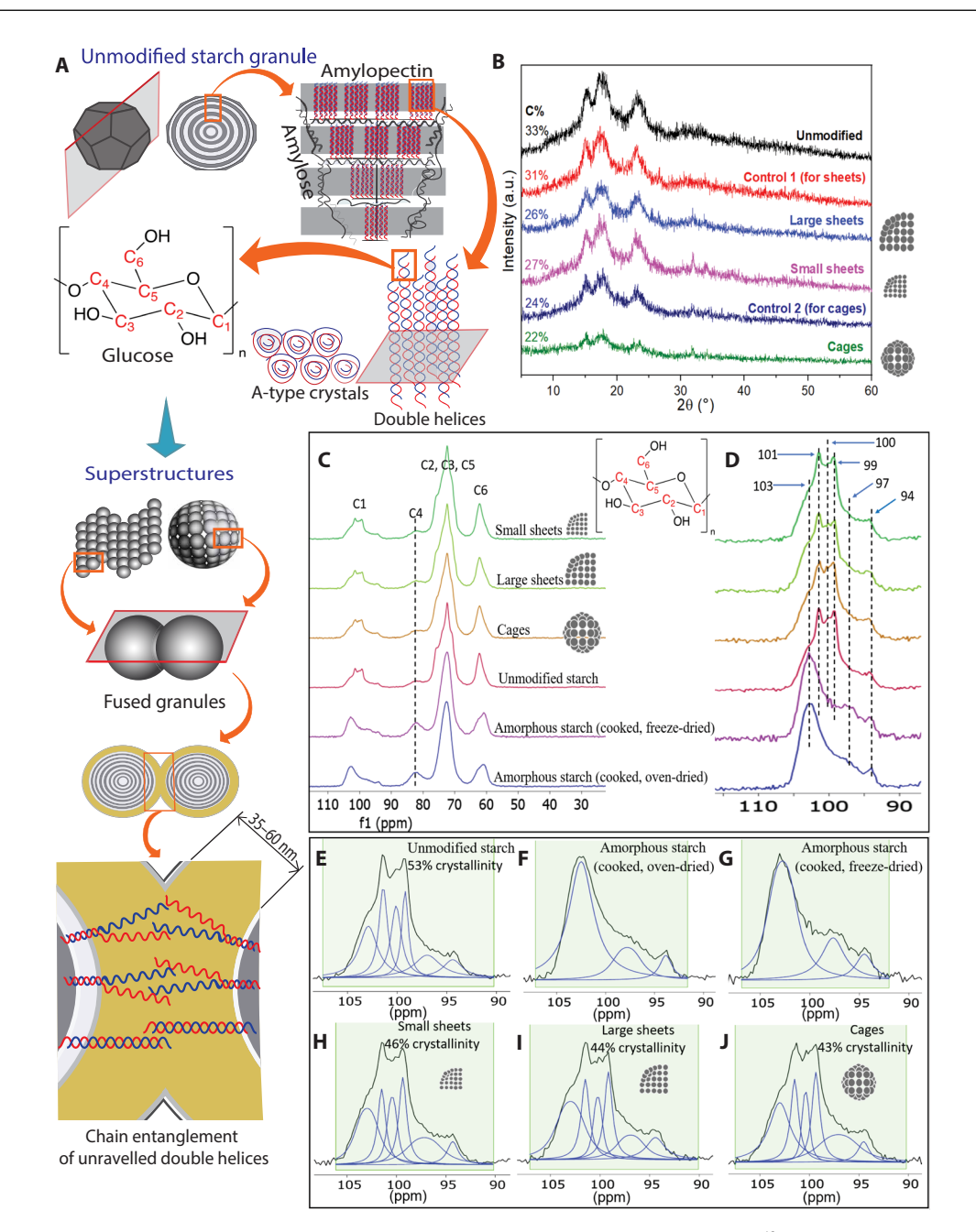


Fig. 5. Structural conformation of starch superstructures: Granular fusion. (A) Molecular fusion schematic; (B) XRD spectra; (C) ¹³C CP/MAS NMR spectra; (D) expanded ¹³C CP/MAS NMR subspectra for the C1 peak for the small sheets, large sheets, hollow cages, and respective controls.

>65% of the native starch's crystallinity (22% for cages versus 33% for unmodified native starch), and this retention of crystallinity appears to impart strength to the cage structure and prevents collapse. In summary, crystallinity as observed from our XRD data follows this order: unmodified (33%) > small sheets (27%) > large sheets (26%) > cages (22%).

If we approximate the granules as 1-µm spheres, and if the partial loss of crystallinity occurs at the surface first and penetrates the sphere radially to its center, then from the XRD results, we can speculate that the granules making up the sheets and cages may have been partially gelatinized about 35 nm (sheets) and 60 nm (cages) deep from the surface. We believe that it is this softened outer layer of

each granule that creates the bridges or fuses to other granules to form the starch superstructures.

Solid-state CP/MAS ¹³C NMR

While XRD provides information regarding long-range molecular order, we used cross-polarization magic angle spinning ¹³C nuclear magnetic resonance (CP/MAS ¹³C NMR) to investigate short-range molecular order and quantify the molecular structures present (Fig. 5, C and D). The glucose chains inside a starch granule can wrap around themselves as single helices (amylose) or double helices (amylopectin), or they can be randomly oriented (amorphous amylose or amylopectin) (23, 26–28). These polymorphs exhibit different local electron densities around their carbon atoms: In the presence of an

external magnetic field, we can tell them apart by their different chemical shifts (27, 29).

The CP/MAS ¹³C NMR spectrum of unmodified starch shows a broad C1 peak [94 to 105 parts per million (ppm)] that can be deconvoluted into six peaks. The three peaks at 94, 97, and 103 ppm are attributed to the amorphous region; while the other three sharper peaks at 99, 100, and 101 ppm are attributed to amylopectin double helices (Fig. 5E) (27). The absence of a distinct peak at ~102 ppm indicates that the amount of amylose single helices is negligible (27). The presence of these sharp peaks is an indication of the crystallinity of the unmodified starch granules.

We found that for fully cooked or amorphous starch, the C1 peak broadens and loses all the sharp peaks that indicate crystallinity (Fig. 5, F and G) (29). Conversely, when starch is only partially gelatinized, as in the case of sheets and cages, the crystalline peaks decrease only slightly, and the amorphous peaks increase (Fig. 5, H to J) (29). Adding together the area under the curve for the deconvoluted sharp peaks and comparing it with the area for the broad peaks, we can estimate the crystallinity of the partially gelatinized starch from amylopectin double helices in this order: unmodified

(53%) > small sheets (46%) > large sheets (44%) > hollow cages (42%) (29).

Combining what we learned from XRD and NMR, we determined that as we fuse starch granules together to form superstructures, we unravel the amylopectin double helices that make up the crystalline regions on the granule surface into random, amorphous coils. In doing so, we disrupt the crystallinity of these granules, reducing it from 33% crystallinity in unmodified starch to 26–27% for sheets and 22% for cages (23). These loosened and unraveled double helices and other amorphous chains entangle with those of adjacent granules via hydrogen bonding, which effectively fuses them together into our sheet and cage superstructures (Fig. 5A).

Structural conformation of starch superstructures: Cross-linking Solid-state ³¹P MAS NMR

After the granules have fused together to form superstructures, we reinforced their fusion by cross-linking their entangled chains with phosphate groups (Fig. 6A). Phosphorus-31 nuclear magnetic resonance (³¹P MAS NMR) shows that the cross-linking agent, sodium

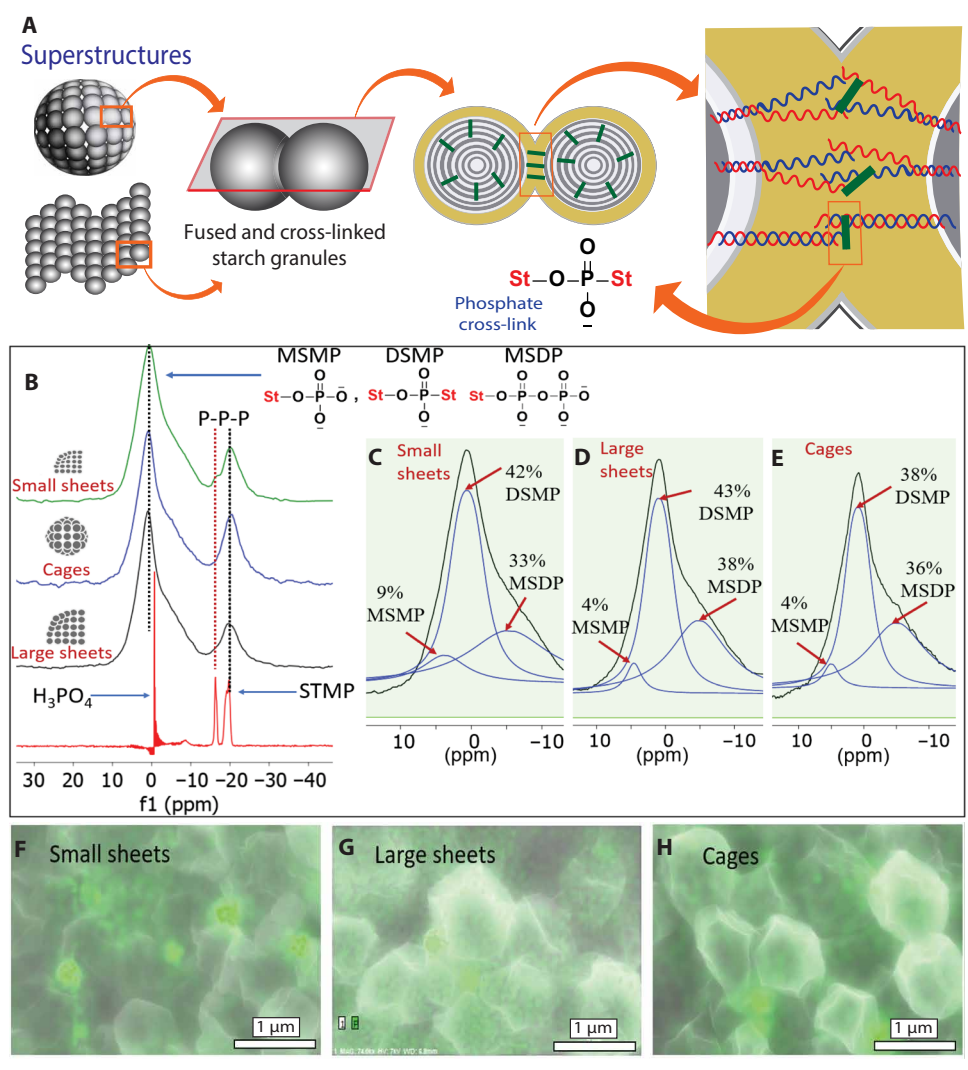


Fig. 6. Structural conformation of starch superstructures: Cross-linking. (A) Molecular cross-linking schematic; (B) ³¹P MAS NMR spectra; deconvoluted ³¹P MAS NMR subspectra of (C) small sheets, (D) large sheets, and (E) cages; SEM-EDX phosphorus density maps of (F) small sheets, (G) large sheets, and (H) cages.

trimetaphosphate (STMP), reacted successfully with starch to form distarch monophosphate (DSMP), monostarch monophosphate (MSMP), and monostarch diphosphate (MSDP), with deconvoluted peaks at 4, 1, and -10 ppm (Fig. 6, B to E) (30). About 15 to 22% of the STMP did not react with starch, either remaining unreacted (peak at -20 ppm) or becoming partially hydrolyzed to triphosphate (TP) (peak at -17 ppm) (30). Only DSMP truly stiches two separate chains together and contributes to cross-linking, while MSMP and MSDP have one arm attached to a chain and a second arm that is unattached. Of all these phosphate forms present, the small sheets, large sheets, and cages contain 42, 43, and 38% as DSMP (30). Coupled with results from phosphorus analysis, we estimate the % crosslinking degree to be 1.9% (small sheets), 2.1% (large sheets), and 1.6% (cages), which is consistent with literature (31, 32). This means that there is one glucose unit that is successfully cross-linked for every 52 (small sheets), 48 (large sheets), and 64 (cages) glucose units in these superstructures, improving their stability.

SEM with energy-dispersive x-ray

While ³¹P MAS NMR and phosphorus analysis gave cross-linking degree, SEM with energy-dispersive x-ray (SEM-EDX) provides additional information on how that cross-linking may be distributed across the surface of these superstructures via phosphorus density maps (Fig. 6, F to H). The intensity of the green color across the different regions of the map indicates how densely populated they are with phosphorus. These maps suggest that cross-linking occurred uniformly across the granules themselves and even more intensely on the fusion bridges between them. The cross-linking reagent may have diffused to the softened, amorphous outer layer of each granule, and as these layers fused or overlapped with each other, more reagent was available to covalently reinforce fusion.

We can summarize the molecular architecture of our superstructures in this way: With partial gelatinization of the starch granules, we are breaking A-type crystals at the outer layer about 35 to 60 nm deep from the surface, which unravels the amylopectin double helices and softens that layer. The unraveled chains in the softened outer layer of one granule then entangles with those of other granules. Cross-linking then covalently reinforces both the granules themselves and the fusion between them by stitching adjacent chains together, boosting the superstructure's stability (Figs. 5A and 6A).

WHC and CCC

WHC measures a thickening material's ability to bind or trap water, which is a good indication of how it would restrict water flow and how effectively it may build viscosity in food (33). When the superstructures are dispersed in water, they stretch out in all directions, forming a network that traps water inside and between them, thus taking up a lot of volume (Fig. 7, A to C). Unmodified, unstructured starch naturally has the lowest WHC, followed by sheets that hold water better, and then by hollow cages that hold the most water (Fig. 7, D and E, black data points). The higher WHC for the small sheets compared to control 1 (P < 0.05) may be due to how these superstructures form multiple layers on top of each other in water, thus trapping water between them. On the other hand, the hollow cavity inside the cages allows for more water to be trapped, which explains why their WHC is about six times that of unstructured, unmodified starch granules (P < 0.05). This value agrees with theoretical calculations: Assuming a loose random packing density of 0.57 (34), a 10-µm-diameter non-hollow cage would contain 298 amaranth starch granules with diameters of 1 μm each, while a

hollow cage of the same diameter would contain only 95 granules. Taking random packing between the hollow cages themselves into account further lowers that number to 95(0.57) = 54 granules. Thus, the theoretical effective volume can be calculated as

Effective Volume
$$\frac{hollow \ cage}{unmodified} = \frac{298}{54} \approx 5.5$$
 (1)

which corresponds well to the experimentally observed spike in the WHC for hollow cages: Hollow cage-structured starch holds about six times more water than the same amount of unstructured starch.

CCC measures the lowest concentration at which a starch dispersion in water forms a nonflowing cake; the lower the CCC, the more effectively a material builds a network to thicken an aqueous dispersion. Our samples showed an inverse trend: As WHC increases, CCC decreases. From unmodified starch to the hollow cage–structured starch (Fig. 7E, red data points), the CCC decreases (P < 0.05), indicating that these superstructures restrict fluid flow better. Whereas unmodified amaranth starch requires a CCC of 24.8% w/w to form a cake, hollow cages form a cake at a CCC of just 5.0% w/w, demonstrating the superior thickening ability of these superstructures.

Viscosity

A higher WHC and lower CCC suggests improved thickening ability for these superstructures; however, the ability of superstructures to hold more water and take up a greater effective volume than unstructured starch may or may not translate to higher viscosity (Fig. 7F). The viscosities of both large and small sheets, for example, overlap with that of control 1 (at shear rate of 1 s⁻¹, where P > 0.05). In the presence of shear, it is possible that these lightly fused sheets break down into their constituent starch granules and therefore have a comparable viscosity to unstructured starch. Hollow cages, on the other hand, exhibited a viscosity that was about one order of magnitude higher than that of the unstructured control 2 (at a shear rate of 1 s⁻¹, where P < 0.05). We attribute this difference to the more tightly fused nature of the hollow cages that allows them to keep their superstructure, hold water inside their cavity, and deliver six times the effective volume of unstructured starch. That hollow cages maintain a viscosity much larger than the control over the entire range of shear rates tested demonstrates their stability. This adds to the body of evidence verifying that these stable superstructures have superthickening abilities.

DISCUSSION

We introduced a platform to make superstructures of different shapes and sizes from carbohydrates. By modulating method parameters, we demonstrated that we can make small sheets, large sheets, and hollow cages, all one amaranth starch granule thick. The granules that compose the sheets are loosely fused together and therefore appear to be fragile. Granules that compose the hollow cages are more tightly fused and are thus more robust and exhibit superthickening abilities. The stability of these starch superstructures depends not only on chain entanglement and cross-linking between partially gelatinized granules but also on each granule retaining a certain level of its native crystallinity, so balance is key.

The potential value of these starch superstructures to the food industry lies in the illusion they provide of there being six times more starch than there really are. Using an alternative superstructure mechanism, as opposed to the classic swelling mechanism of individual granules, hollow cages artificially inflate their volume by holding more water inside their hollow cavities. This in turn inflates their viscosity, which, in foods, may either register as a thicker, richer mouthfeel or allow for lower use levels without compromising texture and taste. For consumers, this could mean reduced-calorie food products to support health. For food manufacturers, this could mean reduced ingredient costs and higher profits. For the global starch supply, which stands at 120 million tons annually, this could

mean effectively increasing that amount sixfold, akin to the proverbial multiplication of loaves, but using science at the micrometer scale the naked eye cannot perceive. This could help ease the enormous strains on our planet and make our lives here more sustainable.

To fully realize the potential of starch superstructures as food ingredients, further work is needed to optimize the platform, including improving starch extraction recovery, and to demonstrate the platform's applicability to other starches and in different food applications.

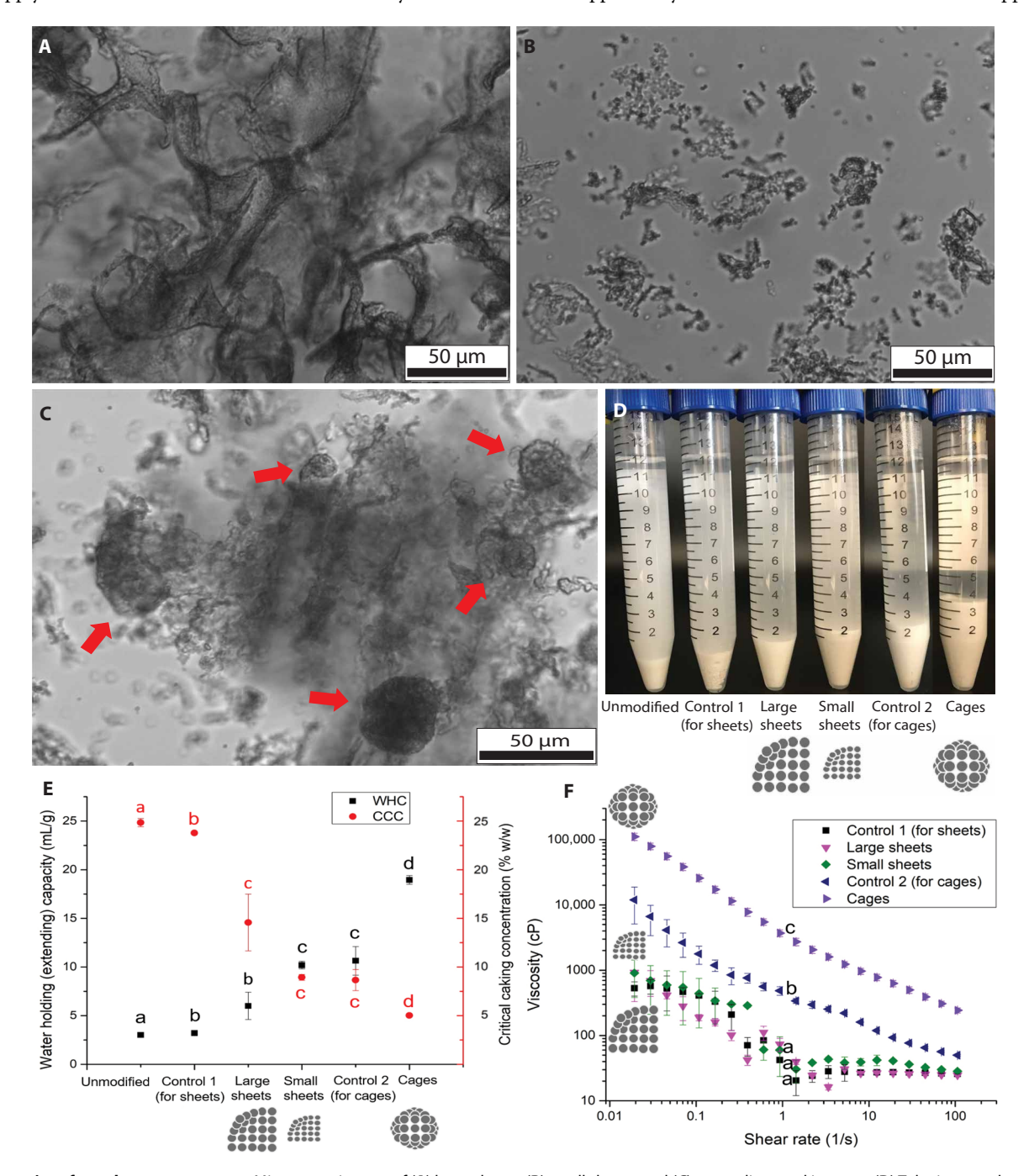


Fig. 7. Properties of starch superstructures. Microscope images of (A) large sheets, (B) small sheets, and (C) cages dispersed in water. (D) Tube images showing water-holding capacity; (E) WHC (black) and CCC (red); and (F) viscosity of unmodified starch, control 1 for sheets, large and small sheets, control 2 for cages, and hollow cages. In (E), data points tagged with different letters are statistically different (P < 0.05); black letters refer to WHC, and red letters refer to CCC. In (F), at a specific shear rate of 1/s, data points tagged with different letters are statistically different (P < 0.05). Error bars refer to SD.

We anticipate that as long as we can extract hydrophobic starch building blocks from flour or grains by retaining enough protein, we can make superstructures from any starch regardless of botanical source and use them as food super-ingredients. Food is a fundamental part of the human experience: What we presented here is a way to make food more thoughtfully through rational design. Because alternate mechanisms are involved, this building-block approach, along with other approaches proposed by our group (35-37), may even offer a path to creating unexplored mouthfeel sensations. If brought to fruition, these superstructures can enrich our lives.

MATERIALS AND METHODS

Materials

Amaranth starch was extracted from a commercial flour. Hydrochloric acid (HCl, 36.5 to 38%, ACS-grade) was obtained from VWR Chemicals (PA, USA). Sodium hydroxide (NaOH, 95 to 100%) was obtained from Thermo Fisher Scientific (NJ, USA). STMP (95%) was obtained from Thermo Fisher Scientific (MA, USA). Sodium sulfate (100.7%) was obtained from J.T. Baker Chemical Co. (NJ, USA). Heptane (99%) was obtained from Sigma-Aldrich (MO, USA).

Extraction of amaranth starch from flour

High-protein amaranth starch was extracted from amaranth flour via an alkaline method our group previously developed that allows us to retain some native proteins (21). Flour (400 g) was added to 2 liters of 0.15% w/v NaOH then mixed at ambient temperature for 1 hour using an overhead stirrer running at 500 rpm. The slurry was filtered for 10 min using a laboratory sieve vibrator (Houghton Manufacturing Co., MI, USA) with a stainless steel 270-mesh sieve. The unfiltered residue was removed from the sieve, added to 400 ml of 0.15% w/v NaOH, mixed for another 10 min, and then resieved for 10 min, adding another 200 ml of 0.15% w/v NaOH to wash out the residue. All filtrates were then collected and centrifuged at 3000g for 20 min, and then the supernatant and the top yellow-brown layer were removed. The white pellet was redispersed in water, the pH adjusted to 6.0 ± 0.1 with 1 N HCl, and the slurry was recentrifuged. The supernatant, together with the top yellow-brown layer, was again removed, and the white pellet was freeze-dried for 24 hours. The dried pellet was then ground using a conical burr grinder. This produced ~50 g of high-protein amaranth starch from amaranth flour (flour contains approximately 54% starch), giving an estimated recovery of 23% of total starch. Note: The high-protein amaranth starch extracted using this method has a particle size of ~1 µm and a protein content of 2.4%, while commercially available starches will have the same particle size but will typically have ≤0.5% protein. This higher protein content facilitates emulsification and subsequent formation of superstructures.

Synthesis of small (<10 $\mu\text{m})$ and large (>10 $\mu\text{m})$ sheets from starch

A schematic of the method used to synthesize large and small sheets is shown in Fig. 2A. First, 0.15 g of STMP and 0.30 g of sodium sulfate were dissolved in 200 ml of deionized (DI) water. Separately, 6 g of starch was added to 40 ml DI water and sonicated for 10 min. The two solutions were then mixed, and the pH was adjusted to pH 10 using 0.15 w/v % NaOH. Then, 10 ml of heptane was added to 20 ml of this mixed solution (In sum, this dispersion is approximately a 30% v/v heptane/water mixture with 0.05 g amaranth starch/ml

heptane and 2.5% w/w STMP/starch.). The mixture was homogenized for 4 min at 22 k rpm (to make small sheets) or 11 k rpm (to make large sheets) using a high-speed homogenizer (IKA T25 digital Ultra Turrax, Germany) and a S25N-18G dispersing tool. This produced a Pickering O/W emulsion with starch at the O/W interface. Next, the emulsions were immersed in liquid nitrogen for 15 min followed by freeze-drying for 2 days to remove heptane and water. The dried powder was then cross-linked in a forced-draft oven at 130°C for 2 hours then cooled. Control 1 was prepared using the same procedure but without the emulsification/homogenization step. All samples were stored in a vacuum desiccator for 24 hours before analysis.

Synthesis of hollow cages (~10 μm) from starch

A schematic of the method used to synthesize hollow cages is shown in Fig. 2A. First, 0.15 g STMP and 0.30 g sodium sulfate were dissolved in 200 mL DI water. Separately, 6 g of starch was added to 40 mL DI water and sonicated for 10 min. The two solutions were then mixed, and the pH was adjusted to pH 10 using 0.15 w/v % NaOH. Then, 10 mL of heptane was added to 20 mL of this mixed solution (In sum, this dispersion is approximately 33 v/v % heptane/ water mixture with 0.05 g amaranth starch/mL heptane and 2.5% w/w STMP/starch.). The mixture was homogenized for 4 min at 22 k rpm using a high-speed homogenizer and a S25N-18G dispersing tool. This produced a Pickering O/W emulsion with starch at the O/W interface. Next, the emulsion was transferred into a 15-ml centrifuge tube (~17-mm diameter) and was heated in a water bath at 75°C for 3 min to partially gelatinize the starch cage (i.e., ~2 min for the emulsion to reach 75°C, plus holding at 75°C for 1 min). The heated emulsion was then quickly quenched in liquid nitrogen for 15 min to stop the gelatinization process and then freeze-dried for 2 days to remove heptane and water. The dried powder was then cross-linked in a forced-draft oven at 130°C for 2 hours and then cooled. Control 2 was prepared using the same procedure but without the emulsification/homogenization step. All samples were stored in a vacuum desiccator for 24 hours before analysis.

Scanning electron microscopy

SEM was used to verify that sheets and hollow cages were made and to examine their morphology. The samples were placed on a conductive carbon tape on top of an SEM stub and then dried for 24 hours in a vacuum desiccator. These samples were sputter-coated with gold and viewed under a JCM-6000 Benchtop SEM (JEOL Ltd., Japan) using a secondary electron detector with a 15-kV accelerating voltage at different magnifications. For zoom-in images, samples were coated with carbon using a sputter coater (Denton Desk V, NJ, USA) and then examined with a Zeiss GeminiSEM 500 FE-SEM (Zeiss, Jena, Germany). Objects were scanned with 1 keV and imaged by a high-efficiency secondary electron detector. In addition, to generate phosphorus density maps, EDX images were also taken using a Zeiss 1550 with a Schottky field-emission source and a nanometer-scale electron probe. A Bruker EDX detector was used, with an aperture size of 60 µm and electron beam of 7.0 kV. The Gemini objective lens uses a combined electrostatic/magnetic lens, which serves to reduce the lens aberration and improve the resolution, especially at low voltages.

Estimation of yield for superstructure synthesis

The % yield for making superstructures out of starch was estimated using ImageJ 1.53 t. SEM images of large sheets, small sheets, and

cages were taken at 2000× magnification, with each sample containing a total of 100+ discrete elements. The total area of all structures and particles present in the 2D images were calculated automatically using the software after adjusting the image threshold to capture all structures/particles. Then, the specific superstructure area was calculated after manually identifying the large sheets, small sheets, and intact cages for the respective samples (fig. S2). The % yield was then estimated using the equations below. We note here that because we used 2D images (area) to evaluate 3D superstructures (volume), the % actual yield may deviate from our estimated value. In addition, to get a more accurate estimate of the % yield for cages, we calculated both a minimum and maximum yield. The minimum cage yield is based on the ratio of the total 2D area of intact cages over all structures and particles present. The maximum cage yield is based on the fact that hollow cages can be approximated as hollow spheres, which means that the 2D area can be converted into a 3D spherical surface area using a geometric factor.

% Yield (Large or small sheets) =
$$\frac{A}{C} \times 100\%$$
 (2)

% Yield minimum (Cages) =
$$\frac{B}{C} \times 100\%$$
 (3)

% Yield maximum (Cages) =
$$\frac{B}{C+3B} \times \frac{4\pi r^2}{\pi r^2} \times 100\%$$
 (4)

where A = Total area of sheets (large or small), B = Total area of intact cages, and C = Total area of all structures and particles.

X-ray diffraction

To determine the extent of starch gelatinization and type of crystal arrangement within these superstructures, XRD pattern analysis was performed on the unmodified amaranth starch, small sheets, large sheets, hollow cages, and controls 1 and 2 using a Bruker D8 Advance ECO powder diffractometer (Billerica, MA). The readings were taken from 5° to 60° using a continuous scan and a step size of 0.026 with 20 min^{-1} . Using OriginPro 9.9.0.225, the relative crystallinity (C%) was then calculated using the equation below (38, 39)

Relative crystallinity (C%) =
$$\frac{A_c}{(A_c + A_a)} \times 100\%$$
 (5)

where A_c and A_a are the total areas for the crystalline and amorphous peaks, respectively. In addition, we estimated how deep from the surface (in nanometers) the granules were gelatinized using the equation below. We approximated an amaranth granule as a 1- μ m sphere and assumed that gelatinization starts from the granule surface and proceeds to the center.

Granule depth of gelatinization (in nm) =
$$500 \left(1 - \sqrt[3]{\frac{C\%_{\text{Superstructure}}}{C\%_{\text{Unmodified}}}} \right)$$
(6)

where $C\%_{\text{Superstructure}}$ is the relative crystallinity of the large sheets, small sheets, or cages, and $C\%_{\text{Unmodified}}$ is the relative crystallinity of unmodified starch.

Solid-state NMR

Solid-state ¹³C CP/MAS NMR and solid-state ³¹P MAS NMR measurements were recorded by a DSX-500 Bruker (11.7 T) operating at

125.8 MHz for the ¹³C nucleus and 202.5 MHz for the ³¹P nucleus. A 4-mm Bruker MAS NMR probe was used for the measurement, and TMS and H₃PO₄ were used as the chemical shift references for solid-state ¹³C CP/MAS NMR and ³¹P MAS NMR, respectively. For all measurements, spinal ¹H-decoupling (two-pulse phase-modulated) was applied during signal acquisition. ¹³C CP/MAS NMR samples were run with a spinning rate of 10 kHz, a cross-polarization contact time of 0.5 ms, and a recycle delay of 2 s. ³¹P MAS NMR spectra were acquired with a 12 KHz spinning rate, 4 ms contact time, and 12 s recycle delay. MestReNova software was then used for both the ¹³C and ³¹P NMR subspectra to deconvolute the peaks and integrate the peak areas. Alongside the preparation of the superstructure samples, two amorphous controls were also prepared by cooking 1% w/v unmodified amaranth starch in water for 25 min at 95°C and then drying either by freeze-drying or in a vacuum oven at 60°C for 48 hours. All samples, both superstructures and controls, were then placed in a desiccator containing a saturated solution of K₂CO₃ at 20°C (relative humidity 44%) for 48 hours before analysis.

Phosphorus analysis by ICP spectroscopy

The total phosphorus content $\%P_{\text{total}}$ (dry basis) was measured to estimate the cross-linking. The cages, large sheets, small sheets, and unmodified amaranth starch (blank control) (0.5 g each) were first predigested at ambient temperature for 10 min with 8 ml of concentrated nitric acid (HNO₃) and 2 ml of concentrated hydrochloric acid (HCl) and then an additional 10 min with 1 ml of 30% hydrogen peroxide (H₂O₂). After the predigestion was complete, the samples were then digested using a CEM Microwave Accelerated Reaction System (MARS6) with MarsXpress Temperature Control using 50-ml calibrated Xpress Teflon PFA vessels with Kevlar/fiberglass insulating sleeves. The microwave digestion was conducted in two stages: Stage one was a 10-min ramp to 135°C and a hold for 3 min at 1500 W. Stage two was a 12-min ramp to 200°C and a hold for 15 min at 1600 W. Vessels were brought to 50-ml volume, and the aliquot was then analyzed using a Thermo iCAP Pro XP inductively coupled plasma (ICP) radial spectrometer.

% Cross-linking degree

The % cross-linking degree was calculated from the total phosphorus content by ICP after using a ³¹P NMR correction factor. NMR was used to disambiguate between the actual cross-linked form of phosphate, DSMP, versus non–cross-linked forms such as MSMP, MSDP, triphosphate (TP), and unreacted reagent (STMP). The cross-linking degree was estimated from the following equations

$$\%P_{\text{cross-link}} = \frac{(\%DSMP) \times \%P_{\text{total}}}{(\%DSMP) + (\%MSMP) + (\%MSDP \times 2) + [(\%STMP + \%TP) \times 3]}$$
(7)

$$\% Cross-linking degree = \frac{2 \times M_{\text{starch}} \times \% P_{\text{cross-link}} \times 100\%}{(M_P \times 100) - (M_{PO_4} \times \% P_{\text{cross-link}})}$$
(8)

where % P_{total} is total % phosphorus (dry basis) from ICP; % $P_{\text{cross-link}}$ is the corrected % phosphorus based on ³¹P NMR; % DSMP, % MSMP, % MSDP, % STMP, and % TP are molar percentages from ³¹P NMR; $M_P = 31$, the molar mass of phosphorus; $M_{\text{starch}} = 162$, the molar mass of a glucose unit of starch; and $M_{PO4} = 96$, the molar mass of a cross-linking phosphate bridge.

Optical microscopy

To visualize how the hollow cages, large sheets, and small sheets orient themselves in water, they were dispersed in water (0.1% w/v), mixed for 10 min using a vertical rotator, and then imaged using an Olympus BX51 microscope (MA, USA).

WHC and CCC

To determine how much water these superstructures can hold inside them and between them, and what this could mean for their thickening ability, WHC and CCC were measured. The water-holding capacity of the unmodified amaranth starch, small sheets, large sheets, hollow cages, and controls 1 and 2 were taken as follows: First, empty 15-ml centrifuge tubes were weighed. Then, a 0.2-g amount of the sample powder was dispersed in 12-ml of DI water inside the centrifuge tubes, the samples were vortexed for 1 min, mixed for 10 min in a vertical rotator, and then placed upright and allowed to settle overnight. The supernatant was then removed using a pipet. The wet sediment and the tube were weighed, and then freeze-dried for 24 hours to remove the water being held. The tube and sample were weighed again. The water-holding capacity, and conversely, the CCC were calculated using the following equations (40)

$$Water-holding \ capacity = \frac{wt \ of \ wet \ sediment - wt \ of \ dried \ sediment}{wt \ of \ dried \ sediment}$$

$$(9)$$

Critical caking concentration =
$$\frac{wt \text{ of dried sediment}}{wt \text{ of wet sediment}} \times 100\%$$
 (10)

Viscosity

To determine the actual thickening abilities of these superstructures, the viscosity of 12.5% w/w dispersions of the unmodified amaranth starch, large sheets, small sheets, hollow cages, and controls 1 and 2 were measured using a TA DHR3 rotational rheometer (DE, USA). A 20-mm parallel plate was used, with a 500- μ m gap size. The starch dispersions were vortexed for 1 to 2 min and then mixed for 20 to 30 min in a vertical rotator before measurement. The viscosity was then measured through a 0.02 to 100 s $^{-1}$ shear rate sweep at 25°C.

Effect of heating temperature on cage crystallinity and morphology

The effect of heating temperature on cage crystallinity was investigated by using the method in Fig. 2A with a 3-min heating time but changing the heating temperature to 70°, 72°, 75°, 77°, 80°, and 82°C. The SEM, XRD pattern, and relative crystallinity of these samples were generated using the same methods as above.

Effect of heating time on cage crystallinity and morphology

The effect of heating time on cage crystallinity was investigated by using the method in Fig. 2A with a 75°C heating temperature, but changing the heating time to 0, 2, 2.5, 3, 3.5, 4, and 5 min. The SEM, XRD pattern, and relative crystallinity of these samples were generated using the same methods as above.

Statistics

Triplicate analyses were conducted, unless where otherwise noted. Analysis of variance (ANOVA) and t tests (P < 0.05) were conducted using Microsoft Excel.

Supplementary Materials

This PDF file includes: Sections S1 and S2 Figs. S1 and S2 References

REFERENCES AND NOTES

- J. Bradbury, Nature's nanotechnologists: Unveiling the secrets of diatoms. PLoS Biol. 2, e306 (2004).
- Z. H. Aitken, S. Luo, S. N. Reynolds, C. Thaulow, J. R. Greer, Microstructure provides insights into evolutionary design and resilience of Coscinodiscus sp. frustule. *Proc. Natl. Acad. Sci.* 113, 2017–2022 (2016).
- H. W. Kroto, J. R. Heath, S. C. O'Brien, R. F. Curl, R. E. Smalley, C60: Buckminsterfullerene. Nature 318, 162–163 (1985).
- Y. Shang, Z. Liu, J. Dong, M. Yao, Z. Yang, Q. Li, C. Zhai, F. Shen, X. Hou, L. Wang, N. Zhang, W. Zhang, R. Fu, J. Ji, X. Zhang, H. Lin, Y. Fei, B. Sundqvist, W. Wang, B. Liu, Ultrahard bulk amorphous carbon from collapsed fullerene. *Nature* 599, 599–604 (2021).
- T. Baati, F. Bourasset, N. Gharbi, L. Njim, M. Abderrabba, A. Kerkeni, H. Szwarc, F. Moussa, The prolongation of the lifespan of rats by repeated oral administration of [60] fullerene. *Biomaterials* 33, 4936–4946 (2012).
- Y. Cao, V. Fatemi, S. Fang, K. Watanabe, T. Taniguchi, E. Kaxiras, P. Jarillo-Herrero, Unconventional superconductivity in magic-angle graphene superlattices. *Nature* 556, 43–50 (2018).
- J. de Boer, H. Aiking, On the merits of plant-based proteins for global food security: Marrying macro and micro perspectives. Ecol. Econ. 70, 1259–1265 (2011).
- H. Kahleova, R. Fleeman, A. Hlozkova, R. Holubkov, N. D. Barnard, A plant-based diet in overweight individuals in a 16-week randomized clinical trial: Metabolic benefits of plant protein. *Nutr. Diabetes* 8, 1–10 (2018).
- Y.-J. Lin, P. Punpongsanon, X. Wen, D. Iwai, K. Sato, M. Obrist, S. Mueller, FoodFab: Creating Food Perception Illusions using Food 3D Printing in *Proceedings of the 2020 CHI Conference on Human Factors in Computing Systems (CHI '20)* (Association for Computing Machinery, 2020), pp. 1–13.
- S. Shen, A. J. Hoffman, S. E. Butler, Method of Producing Salt Composition U.S. Patent US20160183573A1 (2016).
- H. S. Joyner, R. A. Wicklund, C. M. Templeton, L. G. Howarth, S.-S. Wong, M. Anvari,
 J. K. Whaley, Development of starch texture rheological maps through empirical modeling of starch swelling behavior. *Food Hydrocoll.* 120, 106920 (2021).
- F. Zhu, Starch based Pickering emulsions: Fabrication, properties, and applications. Trends Food Sci. Technol. 85, 129–137 (2019).
- C. C. Berton-Carabin, K. Schroën, Pickering emulsions for food applications: Background, trends. and challenges. Annu. Rev. Food Sci. Technol. 6, 263–297 (2015).
- L. Chen, F. Ao, X. Ge, W. Shen, Food-grade pickering emulsions: Preparation, stabilization and applications. Molecules 25, 3202 (2020).
- A. Sarkar, E. Dickinson, Sustainable food-grade Pickering emulsions stabilized by plant-based particles. Curr. Opin. Colloid Interface Sci. 49, 69–81 (2020).
- C. Li, Y. Li, P. Sun, C. Yang, Pickering emulsions stabilized by native starch granules. Colloids Surf. A Physicochem. Eng. Asp. 431, 142–149 (2013).
- S. Tao, H. Jiang, S. Gong, S. Yin, Y. Li, T. Ngai, Pickering emulsions simultaneously stabilized by starch nanocrystals and Zein Nanoparticles: Fabrication, characterization, and application. *Langmuir* 37, 8577–8584 (2021).
- T. Ngai, S. A. F. Bon, in Particle-Stabilized Emulsions and Colloids: Formation and Applications (Royal Society of Chemistry, 2014).
- A. Marefati, M. Bertrand, M. Sjöö, P. Dejmek, M. Rayner, Storage and digestion stability of encapsulated curcumin in emulsions based on starch granule Pickering stabilization. Food Hydrocoll. 63, 309–320 (2017).
- J. D. Hoyos-Leyva, L. A. Bello-Perez, J. E. Agama-Acevedo, J. Alvarez-Ramirez,
 L. M. Jaramillo-Echeverry, Characterization of spray drying microencapsulation of almond oil into taro starch spherical aggregates. *LWT.* 101, 526–533 (2019).
- A. Kierulf, J. Whaley, W. Liu, M. Enayati, C. Tan, M. Perez-Herrera, Z. You, A. Abbaspourrad, Protein content of amaranth and quinoa starch plays a key role in their ability as Pickering emulsifiers. Food Chem. 315, 126246 (2020).
- M. Salimi, B. Channab, A. El Idrissi, M. Zahouily, E. Motamedi, A comprehensive review on starch: Structure, modification, and applications in slow/controlled-release fertilizers in agriculture. Carbohydr. Polym. 322, 121326 (2023).
- A. Buléon, P. Colonna, V. Planchot, S. Ball, Starch granules: Structure and biosynthesis. Int. J. Biol. Macromol. 23, 85–112 (1998).
- X. Xia, G. Li, F. Liao, F. Zhang, J. Zheng, J. Kan, Granular structure and physicochemical properties of starches from amaranth grain. *Int. J. Food Prop.* 18, 1029–1037 (2015).
- R. Bhosale, R. Singhal, Effect of octenylsuccinylation on physicochemical and functional properties of waxy maize and amaranth starches. *Carbohydr. Polym.* 68, 447–456 (2007).
- L. Kong, C. Lee, S. H. Kim, G. R. Ziegler, Characterization of starch polymorphic structures using vibrational sum frequency generation spectroscopy. J. Phys. Chem. B 118, 1775–1783 (2014).

SCIENCE ADVANCES | RESEARCH ARTICLE

- I. Tan, B. M. Flanagan, P. J. Halley, A. K. Whittaker, M. J. Gidley, A method for estimating the nature and relative proportions of amorphous, single, and double-helical components in starch granules by 13C CP/MAS NMR. Biomacromolecules 8, 885–891 (2007).
- K. Dome, E. Podgorbunskikh, A. Bychkov, O. Lomovsky, Changes in the crystallinity degree of starch having different types of crystal structure after mechanical pretreatment. *Polymers* 12, 641 (2020).
- C. Mutungi, L. Passauer, C. Onyango, D. Jaros, H. Rohm, Debranched cassava starch crystallinity determination by Raman spectroscopy: Correlation of features in Raman spectra with X-ray diffraction and 13C CP/MAS NMR spectroscopy. Carbohydr. Polym. 87, 598–606 (2012).
- Y. Sang, O. Prakash, P. A. Seib, Characterization of phosphorylated cross-linked resistant starch by 31P nuclear magnetic resonance (31P NMR) spectroscopy. *Carbohydr. Polym.* 67, 201–212 (2007).
- N. da Silva Miranda Sechia, P.T. Marquesa, Preparation and physicochemical, structural and morphological characterization of phosphorylated starch. *Mater. Res.* 20, 174–180 (2017)
- H. Heo, Y.-K. Lee, Y. H. Chang, Effect of cross-linking on physicochemical and in vitro digestibility properties of potato starch. Emir. J. Food Agric. 29, 463–469 (2017).
- S. B. Elhardallou, A. F. Walker, The water-holding capacity of three starchy legumes in the raw, cooked and fibre-rich fraction forms. *Plant Foods Hum. Nutr.* 44, 171–179 (1993).
- G. D. Scott, D. M. Kilgour, The density of random close packing of spheres. J. Phys. Appl. Phys. 2, 863–866 (1969).
- A. Kierulf, M. Azizi, H. Eskandarloo, J. Whaley, W. Liu, M. Perez-Herrera, Z. You,
 A. Abbaspourrad, Starch-based Janus particles: Proof-of-concept heterogeneous design via a spin-coating spray approach. Food Hydrocoll. 91, 301–310 (2019).
- P. Li, A. Kierulf, J. Whaley, J. Smoot, M. P. Herrera, A. Abbaspourrad, Modulating functionality of starch-based patchy particles by manipulating architecture and environmental factors. ACS Appl. Mater. Interfaces 14, 39497–39506 (2022).
- A. Kierulf, M. Enayati, M. Yaghoobi, J. Whaley, J. Smoot, M. Perez Herrera, A. Abbaspourrad, Starch Janus particles: Bulk synthesis, self-assembly, rheology, and potential food applications. ACS Appl. Mater. Interfaces 14, 57371–57386 (2022).

- A. M. Farooq, S. Dhital, C. Li, B. Zhang, Q. Huang, Effects of palm oil on structural and in vitro digestion properties of cooked rice starches. *Int. J. Biol. Macromol.* 107, 1080–1085 (2018)
- X. Kong, S. Kasapis, E. Bertoft, H. Corke, Rheological properties of starches from grain amaranth and their relationship to starch structure. Starch - Stärke 62, 302–308 (2010).
- T.T. B. Ngoc, N.T. Len, J. E. Lindberg, Chemical characterization and water holding capacity of fibre-rich feedstuffs used for pigs in vietnam. Asian-Australas. J. Anim. Sci. 25, 861–868 (2012).
- K. L. Thompson, M. Williams, S. P. Armes, Colloidosomes: Synthesis, properties and applications. J. Colloid Interface Sci. 447, 217–228 (2015).

Acknowledgments: We would like to acknowledge V. Cueva, W. Liu, J. Whaley, M. Perez Herrera, C. Lau, S. Lochtman, and S. Vinarov for technical guidance and support. Thanks are also due to M. Azizi, B. Werner, and P. Carubia for equipment assistance, to M. A. Zamorano for artwork assistance, and to K. J. Donaghy for carefully editing this manuscript. We also acknowledge the use of facilities from the Cornell University Materials Research Science and Engineering Center, and we would also like to thank S. Hwang for access to the Solid State NMR Facility at the California Institute of Technology. Funding: This work received funding from Tate & Lyle Solutions USA LLC and National Science Foundation Materials Research Science and Engineering Center program (DMR-1719875). Author contributions: Conceptualization: A.K., J.S., and A.A. Methodology: A.K., J.L., A.Z., P.L., L.K., J.S., and A.A. Investigation: A.K., J.L., P.L., A.Z., and I.M. Formal analysis: A.K., L.K., J.L., I.M., and A.Z. Funding acquisition: J.S. and A.A. Supervision: J.S. and A.A. Resources: J.S. and A.A. Writing—original draft: A.K., and A.A. Writing—review and editing: A.K., A.Z., J.L., L.K., P.L., I.M., J.S., and A.A. Competing interests: The authors declare that they have no competing interests. Data and materials availability: All data needed to evaluate the conclusions in the paper are present in the paper and/or the Supplementary Materials.

Submitted 12 May 2023 Accepted 18 January 2024 Published 16 February 2024 10.1126/sciadv.adi7069